Mineral Processing

# USING DISCRETE ELEMENT METHOD TO INVESTIGATE BALL MILLING POWER DRAW, LOAD BEHAVIOUR AND IMPACT ENERGY PROFILE UNDER VARIOUS MILLING CONDITIONS

M. B. Kime
*University of Johannesburg*
*Johannesburg, South Africa*
*(Corresponding author: mbkime@uj.ac.za)*

# USING DISCRETE ELEMENT METHOD TO INVESTIGATE BALL MILLING POWER DRAW, LOAD BEHAVIOUR AND IMPACT ENERGY PROFILE UNDER VARIOUS MILLING CONDITIONS


## ABSTRACT

Discrete element method (DEM) modelling has proven over many years to be a powerful tool for studying particulate systems within the mineral processing industry. DEM simulations were conducted to investigate the power draw, load behaviour and impact energy profile of an experimental ball mill under different milling conditions. The variables considered were mill rotational speed (% critical speed), ball size, and lifter face angle. The DEM simulation results indicated that the grinding efficiency would be enhanced by use of 80% critical speed, 30 mm ball diameter, and 45° lifter face angle. These findings can be useful in guiding actual ball milling tests involving an ore sample.



## KEYWORDS

Ball milling, Discrete element method (DEM), Impact energy, Load behaviour, Power draw


## INTRODUCTION

Comminution is a very energy intensive process. It consumes about 5% of the electricity produced worldwide and over 50% of the total energy used in mineral processing plants (Pokrajcic, 2010). Among all comminution stages, ball milling is very energy intensive process. In ball mills, rotational movement provides the rise of the load and the media that are projected and impact on the mill shell at lower angular displacement, resulting in particle breakage. Ball mills are able to reduce particle sizes over a relatively wide range of particle sizes. This explains their wide applicability in the mineral processing industry and research laboratories.

Laboratory ball milling tests coupled with computational simulations using the discrete element method (DEM) have been crucial to enhancing understanding of the effect of operational variables on grinding. Mill rotational speed, size of the grinding media, and lifter face angles and shapes are some of the most important operational variables. DEM has proven over the last decades to be a powerful tool for design and optimization within the mineral processing industry. Examples are numerous, where results obtained from the DEM simulations were valid over a wide range of mill operating conditions (e.g., Mishra & Rajamani, 1992; Cundall & Strack, 1999; Djordjevic, Shi, & Morrison, 2003; Djordjevic, 2005; Kalala, Breetzke, & Moys, 2007; Powell, Weerasekara, Cole, LaRoche, & Favier, 2011).

Many authors have used DEM to investigate the effect of the lifter profile on the charge behaviour and power draw within industrial mills (e.g., Powell, 1991; Cleary, 2001). Lifters play the key primary role in ball milling of giving the best energy transmission to the load and the media when the mill is rotating. Cleary (2001) investigated the influence of lifter shape on charge motion of a 5 m diameter semi-autogenous grinding (SAG) mill using two-dimensional (2D) DEM modelling. Makokha & Moys (2006) assessed the effect of two lifter profiles on the load behavior using three-dimensional 3D DEM. The PFC3D (Itasca Consulting Group, Inc.) DEM simulation model was calibrated to mimic the environment inside an experimental ball mill. The simulated results agreed with the results from their milling tests carried out on a mono-size (–600 + 425 μm) quartz material sample. A change in lifter profile design often changes the mill performance and energy requirement. This was experienced at Los Pelambres when the

lifters of a SAG mill were modified from 72 rows with an 8° face angle to 36 rows with a 30° face angle (Powell et al., 2006). This allowed an increase in the power draw and mill throughput, as well as enhancing operational safety. The mill could operate safely at higher steel loads with no increased risk of liner damage. Dahner & Bosch (2010) compared data from several industrial milling operations with DEM simulated results. They showed that the total milling cost and energy consumption could be significantly reduced if the optimization of the lifter profile was previously done by use of the DEM. In the DEM framework, it is possible to assess the effect of mill operational variables (e.g., % critical speed, % ball filling degree, lifter angle, lifter height) on the grinding.

Work has been conducted on a newly designed laboratory scale ball mill at Mintek to identify the effects of milling operating variables (mill rotational speed, ball size, and lifter face angle) on the relative grinding rates of chromite and non-chromite particles of a Platinum Group Metals (PGM) ore sample. Prior to the experimental work, a comprehensive investigation was performed using DEM modelling on the mill power draw, load behaviour, and impact energy profile under different milling conditions. This paper presents and discusses the DEM simulation results.

## DEM MODELLING RATIONAL

DEM is a numerical tool for modelling the behaviour of particulate systems. Its mathematical fundamentals rely on the knowledge of the contact forces applied on a given particle (particle – particle contact and particle – wall contact), and on solving the particle motion equations using Newton's First Law of Motion. The interactions between particles or between particles and mill walls are often modelled using a linear combination of springs, dashpots, and sliders to represent the elastic, viscous and Coulomb type friction components, respectively. The spring accounts for the restorative force component, and it represents the material stiffness (***K***). The dashpot accounts for the damping force component, and is represented by the coefficient of restitution (***e***). The slider accounts for surface interactions and is represented by the coefficient of friction (***μ***). Materials are also assumed to undergo strain and overlapping.

### DEM fundamentals

The DEM considers particles individually and examines their motion and the forces applied to them (Cundall & Strack, 1999). The displacement of particles per time step is calculated according to the Newton's laws of motion. Figure 1 shows the set of forces applied to particles in motion, which include external forces (gravity, drag) and contact forces (elastic normal interaction, damping, friction).

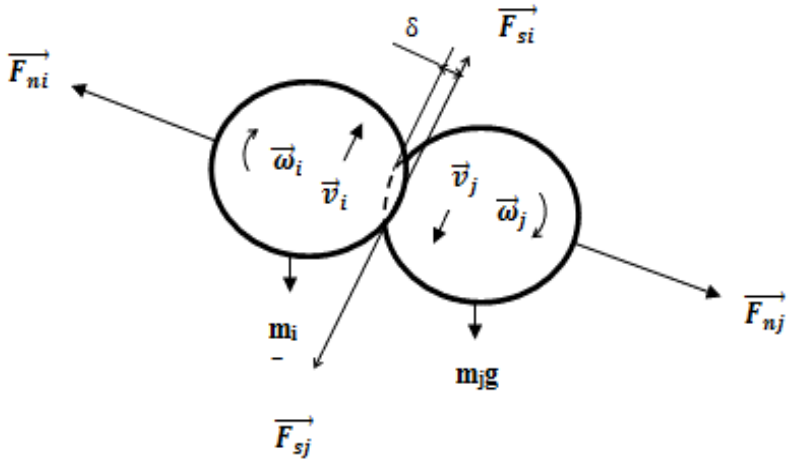


Figure 1. Dynamics of individual particles. Note: **F**, $\boldsymbol{v}$,**ω** and **δ** are the contact force vector, relative linear velocity at the contact, relative angular velocity at the contact and the overlap between particles. The scripts **i** and **j** indicate the two entities in contact; the scripts **n** and **s** indicate the normal and tangential components.

If a linear spring-dashpot model is assumed, the contact force ($F_k$) is given by Equation 1.

$$F_k = K\delta_k - \eta v_k \quad (1)$$

where K [N/m] is the spring constant, δ [m] is the overlap between particles, η is the damping constant, and $\boldsymbol{v}$ [m/S] is the velocity vector.

The total normal force ($F_n$) is given by Equation 2.

$$F_n = -K_n\delta_n + C_n v_n \quad (2)$$

and the total tangential force ($F_s$) is given by Equation 3.

$$F_s = \min\{\mu F_n, K_s \int v_t dt + C_t v_t\} \quad (3)$$

where $C_n$ and $C_t$ are the normal and tangential damping coefficients, respectively. dt is the time step of the simulation. μ is the coefficient of friction.

## DEM SIMULATIONS

### Description of the DEM simulator

The PFC2D (Itasca Consulting Group, 2005) is a generalized MATLAB-based code for DEM purposes. The software offers many options for designing mills with variable lifter face angles, mill speed, mill dimensions, and load volume. In spite of its ability to obtain realistic simulation results, it suffers some obvious shortcomings, mainly due to the expression of the particle flow in two dimensions. This implies that particles can only be circular or disk shaped. Some of these shortcomings are (1) higher strain rate deformation than in real geomaterials (Donzé, Richefeu, & Magnier, 2009), (2) higher packing than in real geomaterials (Cleary & Sawley, 2002; Donzé et al., 2009), (3) lower porosity than real porous materials (Bakunowics & Ecemis, 2014) and (4) use of the average mass properties. These limitations are alleviated in more advanced packages that allow particle flows to be modelled and simulated in three dimensions. In this study, a 2D DEM code was implemented in PFC2D to simulate the ball milling load behaviours. The DEM simulated mill was configured to match the environment inside the laboratory scale ball mill at Mintek. This mill was designed and built for grinding of PGMs. It measured 0.4 m in diameter and had four independent sections of 0.2 m each. It was fitted with 12 lifters spaced circumferentially around the mill shell. It also allowed the use of variable lifter face angles along the mill axial length.

### DEM simulation parameters

The DEM parameters used for the simulations are given in Table 1.

Table 1. DEM parameters used for simulations

| Parameters | Ball-ball contact | Ball-wall contact |
|---|---|---|
| Coefficient of friction | 0.4 | 0.5 |
| Coefficient of restitution | 0.4 | 0.5 |
| Normal stiffness (kN/m) | 400 | 400 |
| Shear stiffness (kN/m) | 300 | 300 |
| Mill speed (% critical speed) | 10–100 | |
| Ball filling, J (%) | 30 | |
| Ball density, ρ, (kg/m$^3$) | 7,800 | |
| Ball size, d, (mm) | 10, 20 and 30 | |

| | | | |
|---|---|---|---|
| Lifter geometry | Trapezoidal | Trapezoidal | Square |
| Number | 12 | 12 | 12 |
| Height (mm) | 15 | 15 | 15 |
| Length (mm) | 400 | 400 | 400 |
| Top width (mm) | 3 | 3 | 20 |
| Bottom width (mm) | 33 | 20 | 20 |
| Face angle (°) | 45 | 75 | 90 |

**Useful information from the DEM simulation**

The first and foremost result of DEM simulation is a picture of actual charge motion. The charge motion image is given by either DEM frames shown in Figure 2 as stills (a) or the particle paths for consecutive frames (b) or by the position density plots (PDPs) (showing the occupancy of any point in the mill by ball centres during a revolution).

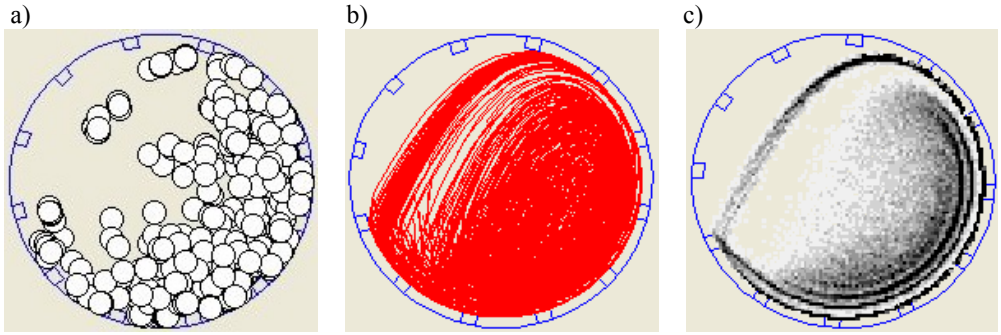


Figure 2. a) DEM frames, b) particle paths for consecutive frames, and c) position density plots (ball diameter = 30 mm)

Additional information that the DEM can deliver is the distribution of the dissipated impact energy spectra of tumbling mills between balls and between balls and lifters. This is very useful to determine the kinetics of the comminution process in the mill and to estimate the grinding effectiveness (King, 2000). Agrawala, Rajamani, Songfack and Mishra (1997) stated that tumbling mill events are efficient when they occur in a region of the mill where the probability of finding an ore particle is higher. Moreover, impact energy should be in the range that can break the ore particle. Very high impact energy is not profitable to the mill as part of it is wasted; rather causing ball and lifter wear than the grinding itself. The impact energy spectra or the distribution of impact energies is obtained by plotting the collision frequency against the collision intensity of ball media on the mill shell. The density of impact energies $d_i$ is the scalar product of the frequency of collisions and the impact energy intensity. The density of impact energies expresses the total mill impact energies at different energy classes. It is expressed by Equation 4:

$$d_i = f_i \times I_i \tag{4}$$

Where $f_i$ is the frequency of collisions (Hz) and $I_i$ is the impact energy (J) and

This function can be conveniently represented in its cumulative form Equation 5:

$$D_j = \sum_{i=1}^{j} f_i I_i \tag{5}$$

$D_j(J)$ gives an idea of the ball milling with accumulation of tumbling impacts.

## RESULTS AND DISCUSSION

### DEM prediction of the mill power draw

The DEM prediction power draw results in Figure 3 show that the power draw was sensitive to lifter face angles at a chosen mill speed. The mill power draw increased gradually as the lifter face angle decreased from 90° to 45°. The mill power draw also increased with increase in rotational speed at lower percent critical speed; but quickly decreased beyond 70–80% of the critical speed. The highest mill power draw corresponded at 80% critical speed, which is in the speed range that most PGM mills are operated. The decrease in the mill power draw was believed to be due to a large proportion of the mill load cataracting at higher speed. This will be further elaborated by examining the PDP snapshots. Further, the mill simulated with 20 mm balls drew high power than the mill simulated with 30 mm balls. This can be explained in that small balls have larger total surface than big balls.

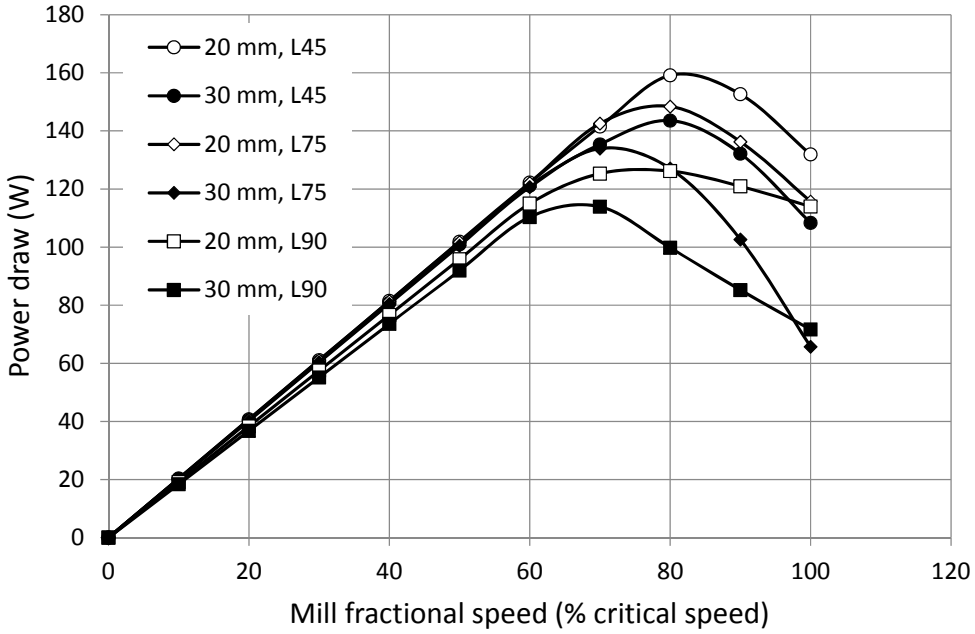


Figure 3. Effects of mill fractional speed and lifter face angle on the mill power draw

In order to validate the power draw prediction by DEM, experimental tests were conducted without any slurry addition to the mill. Only 30 mm steel balls were loaded. The ball filling was set at 30% of the mill volume. The power draw increases gradually as the lifter face angle decreases from 90° to 45°; but quickly decreased beyond 70–80% of the critical speed (Figure 4). The maximum power draw was also reached at different speeds. This is a clear indication that the actual higher speed depends also on the geometry of the lifter used. These results agreed fairly well with the DEM simulation predictions.

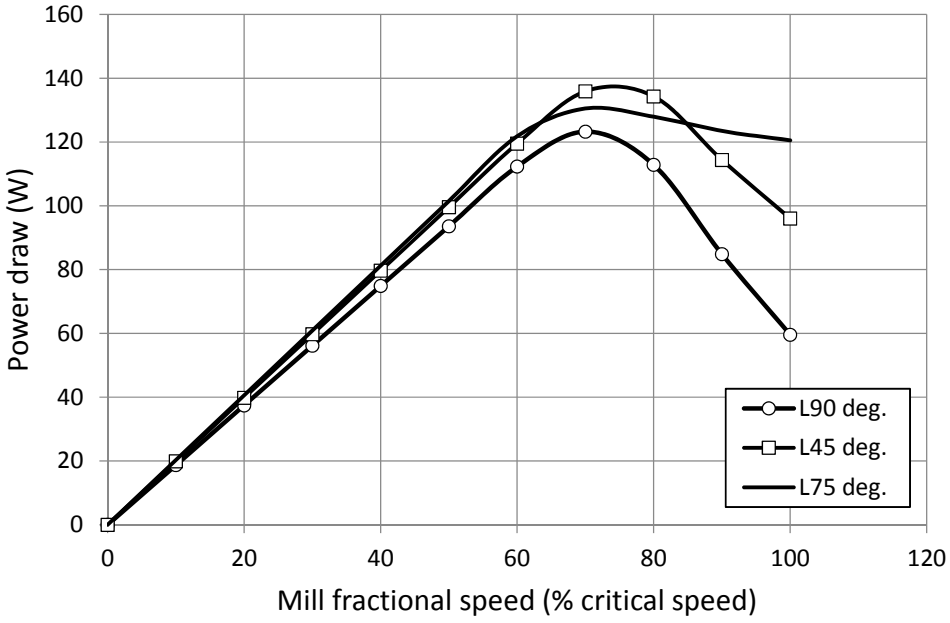


Figure 4. Experimentally measured power

**DEM prediction of the mill load behaviour**

The statistical record of ball positions—referred to as PDPs of balls in motion—was analyzed in order to determine whether different ball sizes exhibited different tumbling behaviours and motions at three different lifter face angles inside the mill. The first two mill revolutions were not important because the mill motion was still unstable. Therefore, the PDP analyses have been considered for three consecutive mill revolutions, starting at the third revolution when the mill was running at steady state conditions.

For each and every frame retained for analysis, a set of axes was superimposed onto the corresponding photograph. With the help of an electronic protractor, the key angular positions (dynamic angle of repose, toe and shoulder positions) of the mill load were accurately measured with the 12 o'clock position being 0° (reference) while the 9 o'clock position was used as 90° (Figure 5).

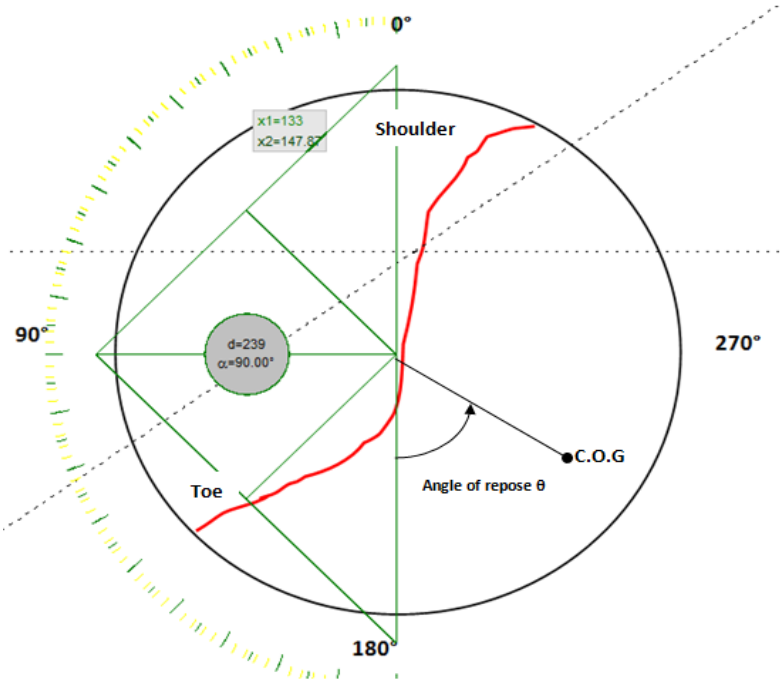


Figure 5. Measuring angles using the MB Ruler protractor

The DEM simulations in Table 2 present the occupancy of any point in the mill by ball centres during a revolution at 75% critical speed. The migration of particles from the cataracting to the cascading zone and vice-versa can be appreciated. Individual motions of particles can also be studied in detail from this type of information. Additionally, the dynamic angle of repose, and the shoulder and toe positions can be accurately measured. It can be seen that for the mill simulated with 90° lifter face angle, cataracting of balls onto the liners is unavoidable. Part of the mill load is thrown far and impact on the mill shell at lower angular displacement. In other words, the energy is returned to the mill as a result of balls being projected to the mill shell. This explains why the mill simulated with 90° lifter face angles drew less mill power. The problem will be enhanced with further increase in mill rotational speed.

Table 2. DEM results showing the occupancy of any point in the mill by ball centres during a revolution at 75% critical speed

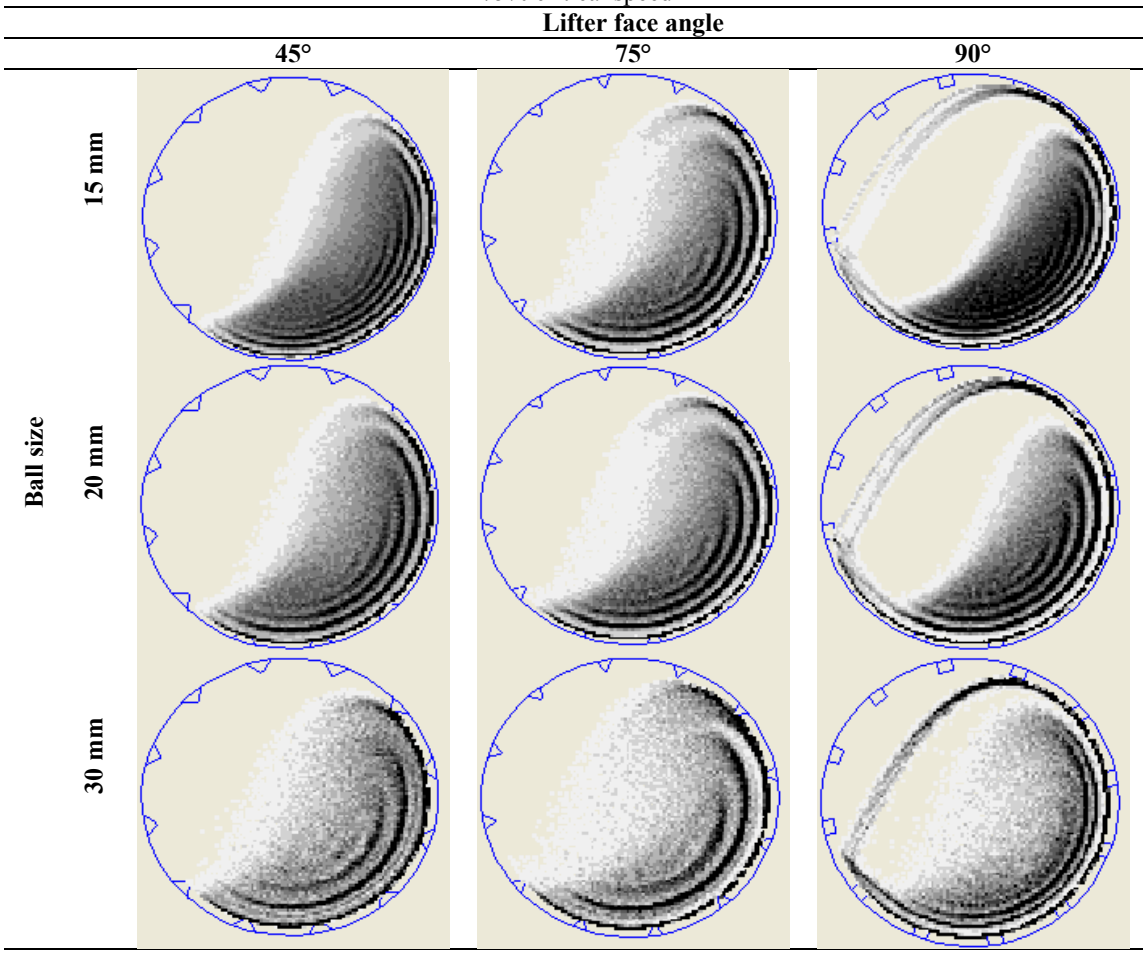


Table 3 compares dynamic angles of repose at various mill speed and lifter face angle. Larger balls exhibited higher dynamic angles of repose compared to smaller balls. This is explained in that there is a larger dynamic (slippage) between large ball layers than smaller ball layers. The dynamic angle of repose also increased with increase in mill speed.

Table 3. Comparison of dynamic angle of repose at different mill speed and lifter face angle

| | | Lifter face angle (°) | | | | | | | | |
|---|---|---|---|---|---|---|---|---|---|---|
| | | 45 | | | 75 | | | 90 | | |
| Ball size (mm) | Mill speed | 65% crit. | 70% Crit. | 75% crit. | 65% crit. | 70% Crit. | 75% crit. | 65% crit. | 70% Crit. | 75% crit. |
| | 15 | 57.1 | 60.5 | 65.0 | 58.5 | 60.1 | 62.9 | 46.4 | 48.3 | 68.1 |
| | 20 | 58.8 | 64.6 | 65.0 | 59.1 | 65.4 | 66.6 | 56.6 | 61.2 | 71.3 |
| | 30 | 59.3 | 65.1 | 65.0 | 60.2 | 63.3 | 63.4 | 65.8 | 66.6 | 72.9 |

The toe and shoulder positions were also analyzed for different mill fractional speed and lifter face angle. Figure 6 shows the results for the mill simulated with 30 mm balls. The shoulder position

increased gradually with the increase in the mill fractional speed, within the mill speed range considered. Conversely, the toe position decreased with the increase in the mill fractional speed. Higher shoulder and lower toe positions were obtained when simulating the mill with the 90° lifter face angle. Therefore, the mill simulated with 90° lifter face angle would have drawn the highest mill power, as might be expected. But, due to a large fraction of balls cataracting and sliding, the mill simulated with 90° lifter face angle drew the least mill power.

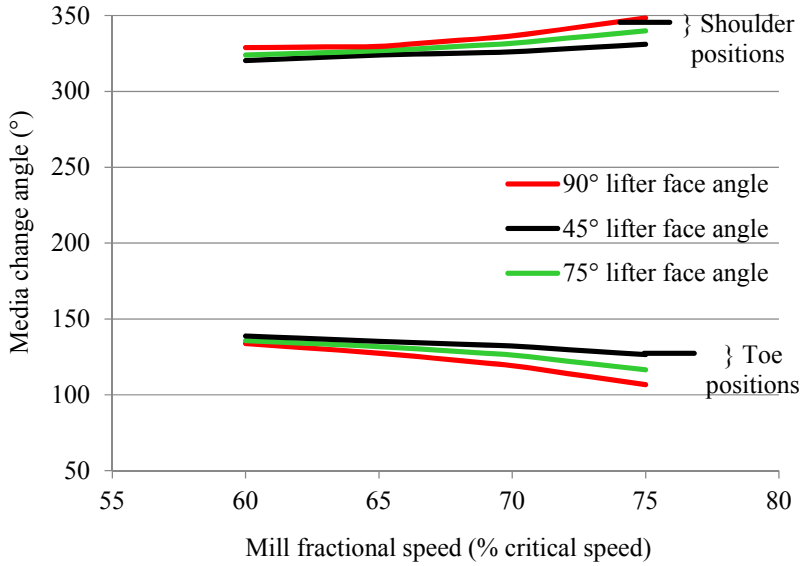


Figure 6. Variations of the toe and shoulder positions of the media charge with the percent fractional speed of the mill

**Impact spectra**

The distribution of the dissipated impact energy spectra of tumbling mills between balls and between balls and lifters was analyzed. The impact energies were less sensitive to change in mill rotational and lifter face angle. However, they strongly depended on the ball size. Figure 7 shows the plots of the frequency of collisions, density of impact energies and cumulative impact energies as a function of the impact classes energy. The impact energy events for the mill simulated with 20 mm balls are located in the lower energy regions as compared to the mill simulated with 30 mm balls. The impact energies were also found to be proportional to the steel ball size weight. The maximum impact energy recorded when using 20 mm balls and 30 mm balls were in the following ratio (Equation 6).

$$\frac{m_{d_{20}}}{m_{d_{30}}} = \frac{\rho d^3_{20}}{\rho d^3_{30}} = \left(\frac{20}{30}\right)^3 = \frac{8}{27} \tag{6}$$

The comparison of the cumulative impact energies curves in Figure 7 shows that the mill simulated with 30 mm exhibited more impact energies than the mill simulated with 20 mm balls. This means that 20 mm balls did not have enough gravitational force to cause major impact energies. That is why it was not useful to represent the impact energies of the mill simulated with 15 mm balls because their spectra were very insignificant. The total cumulative impact energy decreased essentially due to a reduction in events of high energy impact.

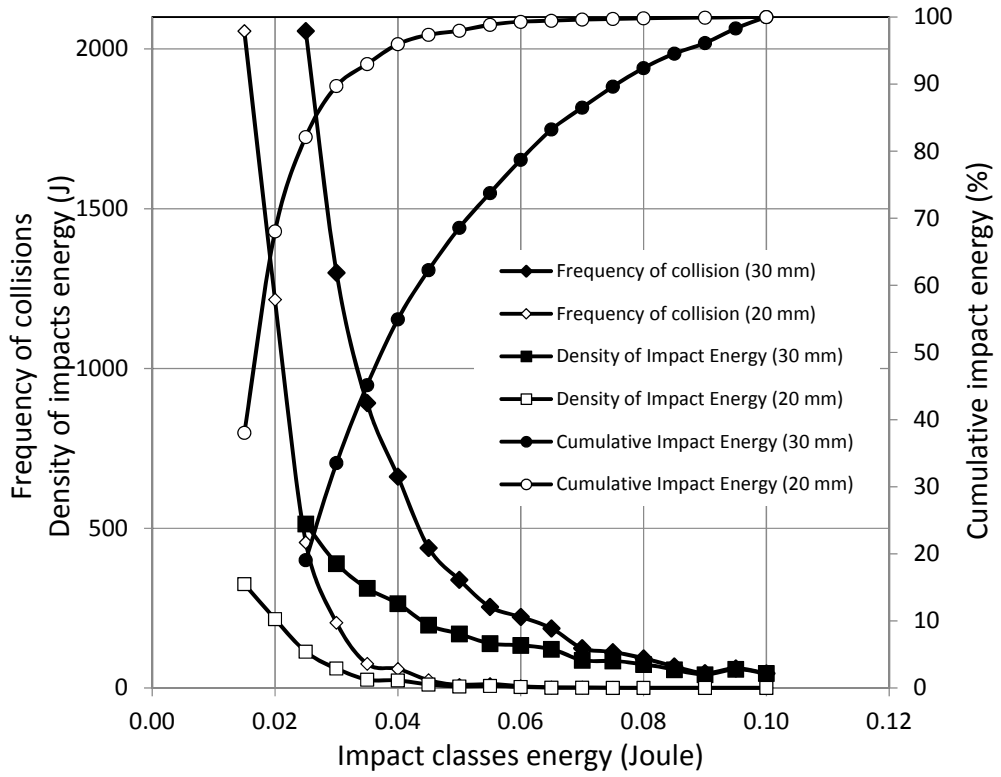

Figure 7. Impact energy spectra as a function of ball size

## CONCLUSIONS

In tumbling ball mills, operational variables such as lifter face angle, ball size and mill rotational speed must be optimized as they affect the dynamic motion of balls, and therefore the mill power draw and the distribution of impact forces. This research used 2D DEM modelling to investigate the effects of mill rotational speed, lifter face angle, and ball size on the mill power draw, load behaviour and the impact energy profile. A simple relationship between the mill power draw and the toe and shoulder positions could not be established. The maximum mill power draw occurred at different toe or shoulder positions, depending on the lifter face angle used. The mill simulated with 90° lifter face angle drew the lowest power, due to a significant proportion of balls cataracting. Some of their momentum was imparted to the mill shell resulting in a loss of power. Also, the mill power draw increased with the mill rotational speed. Irrespective of lifter face angle considered, the peak power draw was between 70 and 80% critical speed. The load behaviour and mill power draw were also strong functions of ball size. Although 2D DEM was used, the results obtained are realistic and valuable in assisting the actual ball milling tests, including an ore sample.

## ACKNOWLEDGMENTS

The author acknowledges the financial support from Mintek for this research work. This work was done partly at Mintek and the DEM simulations were performed at the University of the Witwatersrand. Support from these organizations is acknowledged.

## AUTHOR BIOGRAPHY

Méschac-Bill Kime is a lecturer of Metallurgical Plant at the University of Johannesburg. His research interests include: flowsheeting and optimization of complex process systems, metallurgical process modelling and design, sustainable minerals resource beneficiation.

Mr. Kime holds a BS (Honours) in Metallurgical and Material engineering from the University of Lubumbashi, and an MSc in Chemical Engineering from the University of the Witwatersrand. He is currently a PhD scholar in chemical engineering. He has previously worked as a Metallurgist in a Cu/Co concentrator, smelter and refinery. He consults with industry in the fields of extractive metallurgy and minerals processing.

## REFERENCES


Agrawala, S., Rajamani, R. K., Songfack, P., & Mishra, B. K. (1997). Mechanics of media motion in tumbling mills with 3D Discrete Element Method. *Minerals Engineering*, *10*(2), 215–227

Bakunowics, P., & Ecemis, N. (2014). Validation of porosity in 2D-DEM CPT model using large scale shaking table tests in saturated sands. Oka, M., Murakami, A., Uzuoka, R. and Kimoto, S. (Eds). Computer methods and recent advances in Geomemechanics, pp. 483–488, CRC Press 2014.

Cleary, P. W. (2001). Charge behaviour and power consumption in ball mills: sensitivity to mill operating conditions, liner geometry and charge composition. *International Journal of Mineral Processing, 63*, 79–114.

Cleary, P. W., & Sawley, M. L. (2002). DEM modelling of industrial granular flows: 3D case studies and the effect of particle shape on hopper discharge. *Applied Mathematical Modelling, 26*, 89–111.

Cundall, P. A., & Strack, O. D. L. (1979). A discrete numerical model for granular assemblies. *Geothechnique*, *29*(1), 47–65.

Dahner, J., & Bosch, A. V. (2010). Total primary milling cost reduction by improved liner design. The 4th International Platinum Conference, Platinum in transition 'Boom or Bust', *The Southern African Institute of Mining and Metallurgy*, 2010

Djordjevic, N. (2005). Influence of charge distribution on net-power draw of tumbling mill based of DEM modelling. *Minerals Engineering, 18*, 375–378.

Djordjevic, N., Shi, F. N., & Morrison, R. D. (2003). Applying discrete element modelling to vertical and horizontal shaft impact crushers. *Minerals Engineering, 16*, 983–991.

Donzé, F. V., Richefeu, V., & Magnier, S. A. (2009). Advances in discrete element method applied to soil, rock and concrete mechanics. *Geotech Eng* 8.

Itasca Consulting Group, Inc. (2005). PFC2D user's manual. Minneapolis, MN: Author.

Kalala, J.T., Breetzke, M., Moys, M.H. (2007). Study of the influence of liner wear on the load behaviour of an industrial dry tumbling mill using the Discrete Element Method (DEM). *International Journal of Mineral Processing*, *86*(1/4), 33–39.

King, R. P. (2000). Technical notes 8 grinding

Makokha, A. B., & Moys, M. H. (2006). Effect of cone-lifters on the discharge capacity of the mill product case study of a dry laboratory scale air-swept ball mill. *Minerals Engineering*, *20*, 124–131.

Mishra, B.K. and Rajamani, R.K. (1992). The discrete element method for the simulation of ball mills. *Applied Mathematical Modelling, 16*, 598–604.

Pokrajcic, Z. (2010). A methodology for the design of energy efficient comminution circuits. PhD Thesis. The University of Queensland, 2010.

Powell, M. S. (1991). The design of rotary-mill liners, and their backing materials. *The Southern African Insititute of Mining and Metallurgy, 91*, 63–75.

Powell, M., Smit, I., Radziszewski, P., Cleary, P., Rattray, B., Klas-Goran, E., & Schaeffer, L. (2006). The selection and design of mill liners. Society for Mining, Metallurgy and Exploration, pp. 331-376.

Powell, M., Weerasekara, N. S., Cole, S., LaRoche, R. D., & Favier, J. (2011). DEM modelling of liner evolution and its influence on grinding rate of ball mills. *Minerals Engineering, 24*, 341–351.